

PHOTONIC MODES IN DISPERSIVE AND LOSSY SUPERLATTICES CONTAINING NEGATIVE-INDEX MATERIALS

H. Kinto-Ramírez^{1,*}, M. A. Palomino-Ovando¹, and F. Ramos-Mendieta²

¹Facultad de Ciencias Físico Matemáticas, Benemérita Universidad Autónoma de Puebla, Apartado Postal 1152, Puebla, Puebla 72000, México

²Departamento de Investigación en Física, Universidad de Sonora, Apartado Postal 5-088, Hermosillo, Sonora 83190, México

Abstract—We have calculated the photonic bands of a dispersive and lossy periodic array of left-handed metamaterial layers in air. Depending on the behavior of the fields inside the metamaterial component, two categories of modes for oblique propagation are identified: the *oscillatory* and the *tunneling* modes. In order to characterize these two types of solutions, we calculate the complex photonic bands; a criterion of penetration-limit is introduced to quantify the absorption effects. Our results show that oscillatory TE and TM waves can be excited by light incident from air at low frequencies (within the metamaterial regime). In the region of high frequencies only TE tunneling modes are available. To complement the description of the absorption effects, we present transmission spectra and field profiles for TE waves in finite layered systems for the two types of modes here studied.

1. INTRODUCTION

Left-handed metamaterials (LHMs), or negative-index materials, are a new class of artificial structures with novel optical properties. They are *left* because they can support electromagnetic waves with electric field, magnetic field and wave vector following a left-hand rule. The reason underlying this behavior, discussed initially by Veselago [1], is that these materials have negative index of refraction: within a frequency

Received 29 June 2011, Accepted 10 October 2011, Scheduled 16 October 2011

* Corresponding author: Hector Kinto-Ramírez (275700812@alumnos.fcm.buap.mx).

range these materials display simultaneously negative permittivity and negative permeability. [It is worth mentioning that very interesting remarks on the initial studies of negative refraction were recently pointed out by Agranovich and Gartstein [2]; there exists documentary evidence suggesting that pioneering studies of this phenomenon could have been realized as early as 1940.] Experimentally, the left-hand behavior was demonstrated in microwave regime for a system of splitting resonators interspersed with metallic wires [3].

Once the fundamental properties of the LHMs were known [4–6], it was natural to propose the creation of heterostructures with LHM constituents. For layered structures containing LHMs and ordinary right-handed materials (RHMs), several results have been reported [7–14]. For example, unusual photon tunneling between two semi-infinite media separated by a RHM-LHM bilayer was found in the microwave regime [10]. Also, in calculating the transit time through LHM barriers it was demonstrated that a phase-stationary approximation could be inappropriate because the tunneling effect apparently violates causality [11]. On the other hand, a new type of photonic band gap (not based on interference mechanisms) has been found in LHM/RHM structures associated to the zero value of the averaged refractive index (the zero- \bar{n} gap) [12, 13].

Reference [14] explicitly demonstrates the existence of four types of bulk electromagnetic modes in periodic LHM/RHM arrays: the *spurious modes*, without physical meaning because they exhibit complex frequency, the *discrete modes*, real modes that appear at the center or the border of the Brillouin zone, the *tunneling modes*, characterized by evanescent (decreasing or increasing) fields in subsequent layers, and, the ordinary *propagating* modes. The same electromagnetic modes are expected even when absorption is not ignored [10, 14].

We know that in general, losses attenuate the propagating fields in RHMs or LHMs. In the latter case, however, some authors have addressed a more relevant role of absorption as material property; evanescent amplifying waves in non absorbent metamaterial slabs can drastically change to waves of decaying behavior when losses are taken into account [15]. Consequently, the focusing effect of a LHM slab as a perfect lens, which is one of the most interesting applications suggested for LHMs [4], could be substantially diminished. However, other authors have found that the amplification of pure evanescent waves depends not only on losses, but also on the slab thickness. The final consequence could be that superlensing effect can be achieved even under the presence of small absorption [16].

Losses also play an important role in the optical properties of

multilayer structures with LHM constituents. For example, the very interesting zero- \bar{n} gap that was found in non absorbent photonic systems can disappear, because the absorption modifies the photonic band structure introducing new photonic states inside the gaps [17]. On the other hand, it is possible to control the damping of evanescent amplifying waves in a thick LHM slab by sectioning it in several layers to form a LHM/RHM multilayer. Knowing that the power loss is proportional to the field intensity, the loss effect can be diminished by increasing the number of layers in the multilayer structure but leaving the same total thickness of the original LHM sample [18]. As thinner the LHM layers are, shorter is the enhancement of the field amplitude in each layer and smaller the power loss.

In this paper we study numerically the photon propagation in periodic superlattices of alternated LHM and RHM layers. The main goal is to quantify the role played by the losses. For the LHM component we use dispersive equations for both permittivity and permeability; absorption is included in these expressions and the RHM is air. The projected photonic bands are calculated to identify the frequency regions of modes of oscillatory and tunneling character. Due to the presence of absorption the photonic bands are complex. In describing the fields we introduce a numerical criterion to separate the modes in the bands as a function of their penetration distance. Finally, field profiles and transmission spectra in finite superlattice samples are presented here, establishing a connection with the photonic bands.

In a right-handed system constituted by two semiinfinite media separated by a layered barrier, the tunneling phenomenon involves evanescent fields in the barrier. The incident fields that decay exponentially at least in one of the barrier layers reach the transmitting medium with finite amplitude conveying electromagnetic energy. On the other hand, if a LHM layer is introduced in the barrier, the tunneling phenomenon preserves and the transmitted intensity could be amplified (photons can tunnel a greater distance). The reason of this phenomenon is that a LHM amplifies the evanescent fields. The effect has been clearly discussed in Reference [10]. Here we shall describe the properties of the electromagnetic waves in a periodic LHM/RHM layered structure. We focus the study on the absorption effects on the modes having oscillatory fields in the RHM (air) layers and evanescent or oscillatory fields in the LHM layers. [Throughout this paper we will use the term oscillatory (tunneling) mode for a solution of the wave equation having oscillatory (exponentially decaying/increasing) fields in the LHM layers] We shall see that within the metamaterial regime the waves which are incident from air are more penetrating in the region of high frequencies; they are TE waves of tunneling type.

LHMs are generally modeled using an effective permittivity ε_{eff} and an effective permeability μ_{eff} which involve the absorption parameters γ_e and γ_m , respectively. It is not easy to estimate theoretically the values of these two parameters. However, they have been quantified by comparing very precise numerical simulations with experimental results [6, 19, 20]. An important point is that many authors have assigned the same value for both parameters [6, 21, 22]. Thus, the dissipation factor $\gamma_e = \gamma_m = \gamma$ is seen as an *effective* factor that results from all the possible mechanisms of losses: currents in the metallic components, energy dissipation in LC resonators, and even, due to the complicated structure of the LHM unit cell, scattering of light. For describing the wave propagation in layered LHM/RHM arrays we will assume that ε_{eff} and μ_{eff} are valid for the LHM components. This is possible because the wavelengths associated to the resonances of ε_{eff} and μ_{eff} — that define the lower frequency limit of the metamaterial regime — are much larger than the intrinsic unit cell size. Such approximation remains valid even for LHM slabs of a few cells [12, 23].

The paper is organized as follows: in Section 2 we present the mathematical formalism employed in our calculations. Models for the dispersive parameters of a LHM are discussed. Then in Section 3 the main characteristics of the oscillatory and tunneling modes are analyzed. Transmission spectra as a function of the absorption parameter are shown. Finally in Section 4 the conclusions of the work are given.

2. METHOD OF CALCULATION

For describing the LHM layers we take into account dispersive and lossy effects employing the frequency dependent permittivity and permeability functions given by [24]

$$\varepsilon(\omega) = 1 - \frac{\omega_p^2}{\omega^2 + i\gamma\omega}, \quad \mu(\omega) = \frac{\omega^2 - \omega_b^2}{\omega^2 - \omega_0^2 + i\gamma\omega}. \quad (1)$$

The parameters have the values: $\omega_{p,b,0} = 2\pi f_{p,b,0}$; $f_p = 12$ GHz; $f_b = 6$ GHz; $f_0 = 4$ GHz and γ can be chosen as high as $\gamma = 0.1\omega_0$. In Figure 1 we plot the respective real and imaginary components of $\varepsilon(\omega)$ and $\mu(\omega)$. As can be seen the metamaterial frequency regime is defined by the frequency range where $\text{Re}(\mu)$ is negative. [For the value of the absorption parameter γ we are following the criteria of several authors. In Reference [6], for example, the theory-experiment matching required $\gamma' = 1$ GHz when the LC resonance $f_0 = 10.5$ GHz. Thus the absorption parameter can be as high as $\gamma' = 0.1f_0$].

We consider a system of alternated LHM and RHM layers that is periodic in the z direction. For the photonic band structure and transmission calculations we have employed the well-known matrix transfer method. The unit cell consists of two layers of permittivity, permeability and thickness $\varepsilon_1, \mu_1, d_1$ and $\varepsilon_2, \mu_2, d_2$, respectively. The period of the structure is $a = d_1 + d_2$. The index of refraction of the layers is written as $n_j = \pm\sqrt{\varepsilon_j\mu_j}$, with $j = 1, 2$; the positive (negative) sign corresponds to the RHM (LHM).

The basic relation between the electric and magnetic fields of different layers is written as

$$\begin{pmatrix} E_y \\ H_x \end{pmatrix}_{z=z_N} = M \begin{pmatrix} E_y \\ H_x \end{pmatrix}_{z=z_1}, \quad (2)$$

with the transfer matrix given by $M = m_N m_{N-1} m_{N-2} \dots m_j \dots m_1$ (N is the number of layers) and

$$m_j = \begin{bmatrix} \cos k_{zj} d_j & \frac{i}{Y_j} \sin k_{zj} d_j \\ i Y_j \sin k_{zj} d_j & \cos k_{zj} d_j \end{bmatrix}, \quad (3)$$

where $Y_j = \frac{\varepsilon_j \omega}{c k_{zj}}$ for TM waves and $Y_j = -\frac{c k_{zj}}{\mu_j \omega}$ for TE waves; c is the speed of light and k_{zj} is the component of the wave vector perpendicular to the layers. The electric and magnetic fields are written as

$$E_{yj} = -A_j^+ e^{i k_{zj} z} - A_j^- e^{-i k_{zj} z}, \quad (4)$$

$$H_{xj} = Y_j \left(A_j^+ e^{i k_{zj} z} - A_j^- e^{-i k_{zj} z} \right), \quad (5)$$

In terms of the reflection coefficient r the field amplitudes in any internal layer can be also obtained with the transfer matrix method:

$$A_j^+ = \frac{e^{-i k_{zj} z}}{2 Y_j} \{ (-1-r) (m_{21j} - m_{11j} Y_j) + Y_0 (1-r) (m_{22j} - m_{12j} Y_j) \}, \quad (6)$$

$$A_j^- = \frac{e^{i k_{zj} z}}{-2 Y_j} \{ (-1-r) (m_{21j} + m_{11j} Y_j) + Y_0 (1-r) (m_{22j} + m_{12j} Y_j) \}, \quad (7)$$

In these equations the four matrix components $m_{11j}, m_{12j}, m_{21j}$ and m_{22j} are the components of the 2×2 matrix $M_j = m_j m_{j-1} \dots m_1$. Finally, with the same transfer matrix method we find the reflection coefficient:

$$r = \frac{(-m_{21N} + m_{22N} Y_0) + (-m_{11N} + m_{12N} Y_0) Y_{N+1}}{(m_{11N} + m_{12N} Y_0) Y_{N+1} + (m_{21N} + m_{22N} Y_0)}. \quad (8)$$

Now the matrix components are the four elements of the matrix $M_N = m_N m_{N-1} \dots m_1$.

When both ε_j and μ_j are negative, the sign of the wave vector $k_{zj} = \pm \sqrt{\frac{\omega^2}{c^2} \varepsilon_j \mu_j - \beta^2}$ should be also negative. Afterwards, by applying the Bloch theorem it is easy to obtain the dispersion equation for the periodic system

$$\cos Ka = \frac{m_{11} + m_{22}}{2}. \quad (9)$$

In this equation K is the Bloch wave vector that takes the values of the reduced Brillouin zone, $0 \leq K \leq \pi/a$; $(m_{11}, m_{12}; m_{21}, m_{22})$ is the transfer matrix of the unit cell. Finally the allowed frequency bands for wave propagation satisfy the condition $|\cos Ka| \leq 1$.

In calculating the frequency bands of oblique propagation, the so-called *projected* bands, we must proceed carefully in order to identify the type of modes in the bands. The general relation between the frequency and the wave vector components in the j -th LHM layer is

$$\omega = \frac{c \sqrt{\beta^2 + k_{zjR}^2 - k_{zjI}^2 + 2ik_{zjR}k_{zjI}}}{\sqrt{\varepsilon_j \mu_j}}, \quad (10)$$

where $k_{zj} = k_{zjR} + ik_{zjI}$ is the complex wave vector component in the z direction and β is the real wave vector component in the x direction (β is the same in all the layers). We look for solutions with real frequency. Without losses it is easy to classify the possible electromagnetic modes. Solutions with $k_{zjR} \neq 0$ and $k_{zjI} = 0$ correspond to ordinary oscillatory fields. It means that the superlattice support electromagnetic modes with oscillatory fields in the LHM layers. On the other hand, with $k_{zjR} = 0$ and $k_{zjI} \neq 0$, with $\beta^2 > k_{zjI}^2$, the fields vary exponentially (decreasing/increasing) in the LHM layers; these are the tunneling modes.

It is known that under lossless condition the allowed photonic bands are characterized by a real Bloch wave vector. Nonetheless, when absorption is taken into account, numerical solutions for the wave equation can be found with real frequency but the Bloch wave vector becomes complex, $K = K_r + iK_i$; consequently, the waves will decay exponentially as they penetrate into the superlattice, with penetration distance inversely proportional to K_i . Note the reader that losses make more complex the solutions for Equation (10) because k_{zjR} and k_{zjI} are different than zero simultaneously. Thus, inside a single LHM layer of the superlattice the field amplitude is expected to decrease as the wave penetrates. However, as we mentioned previously, increasing amplitude can also exist particularly for the tunneling modes.

3. NUMERICAL RESULTS

We begin presenting the photonic band structure of the LHM-RHM superlattice described previously. The filling fraction for the LHM is $f = 0.5$. In Figure 1 we find that $0.133 < \omega a/2\pi c < 0.199$ is the metamaterial regime (there exist also, beyond the scale of the figure, the region of opacity, $0.20 < \omega a/2\pi c < 0.40$, and the region of transparency, $\omega a/2\pi c > 0.40$). We focus the study only on the metamaterial regime. Figure 2 shows the TE (right panel) and TM (left panel) projected bands (β, ω) for lossless materials. The darker regions correspond to modes with oscillating fields in the LHM layers. Contrarily, in the light gray regions the fields are evanescent in those layers. Note that for low frequencies the solutions are quite symmetric

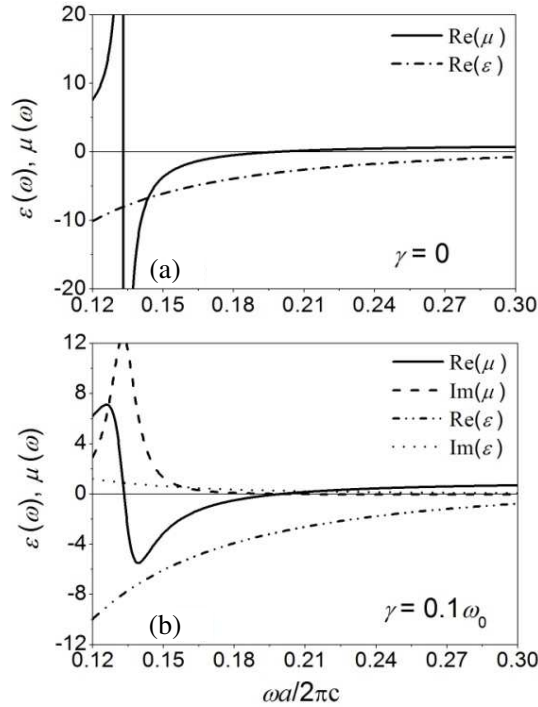


Figure 1. The frequency-dispersive permittivity $\epsilon(\omega)$ and permeability $\mu(\omega)$ functions. With finite loss parameter γ both functions become complex: (a) $\gamma = 0$ and (b) $\gamma = 0.1\omega_0$. The frequency region in which both $\text{Re}(\epsilon)$ and $\text{Re}(\mu)$ are negative is the metamaterial regime.

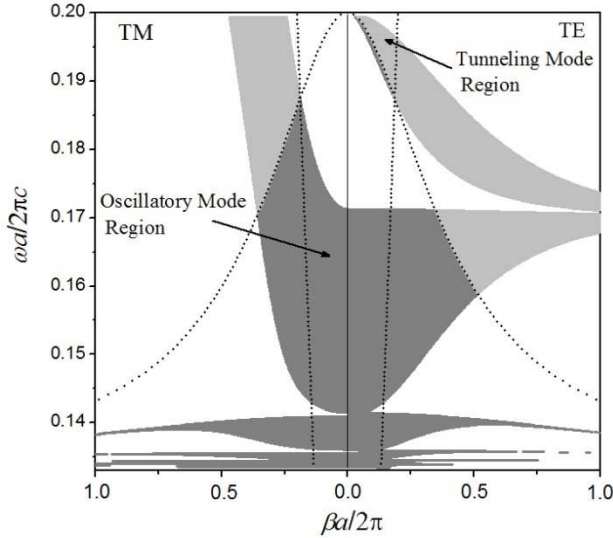


Figure 2. The projected TM and TE photonic bands. The Gaussian-type dotted curve is the metamaterial light-curve. The dotted right lines define the light-cone. For any β value, the borders of the projected bands correspond to the borders of the Brillouin zone. The arrows indicate the two regions inside the light-cone of interest in this work. The darker regions for both TE and TM polarizations correspond to oscillatory modes; the light gray region for TE polarization inside the light-cone contains the tunneling modes.

for both polarizations. In order to define the regions of tunneling modes we are plotting in Figure 2 the vacuum light-line ($\beta = \frac{\omega}{c}$) and the metamaterial light-curve ($\beta = \frac{\omega}{c} \sqrt{\epsilon_m \mu_m}$). In finite samples only the modes inside the light-cone can be excited by light incident from vacuum; outside of the light-cone the fields in the air layers are evanescent. On the other hand, below the metamaterial light-curve the modes are oscillatory in the LHM layers but above this curve the modes acquire evanescent behavior. Thus, with vacuum as incident and transmitting media, the tunneling modes for wave transmission in finite samples are those lying inside the light-cone and above the metamaterial light-curve (See Figure 2).

Figure 2 shows that the photonic bands for wave propagation along the superlattice axis ($\beta = 0$) are, as it must be, the same for TE and TM polarizations. There exist, however, a strong difference

of the solutions for oblique propagation ($\beta \neq 0$): an unusual photonic band defined only for $\beta \neq 0$ arises for TE modes. It is known that in one dimensional photonic crystals of RHM components the projected bands are wider as $\beta \rightarrow 0$ (thinner as $\beta \rightarrow \infty$). The bands on the right panel of Figure 2 show that a RHM/LHM superlattice does not follow this rule in the metamaterial regime. [Parenthetically, it is worth mentioning that for large β the two upper TE bands of Figure 2 converge to the dispersion curve of the surface modes at the air/LHM interface. Such modes appear due to the different permeability of both media [25]. There exist also surface modes for TM waves, but they appear above the scale of Figure 2, in the metallic regime. The topic of surface waves will be not discussed in this paper].

Without losses the borders of the allowed projected bands are defined by the border of the Brillouin zone. In Figure 3 we open artificially the projected bands for TE modes at $\frac{\beta a}{2\pi} = 0.1$ [it is the same Figure 2 but showing the dispersion relation inside the first Brillouin zone for the selected β value]. As expected, the wave vector is real

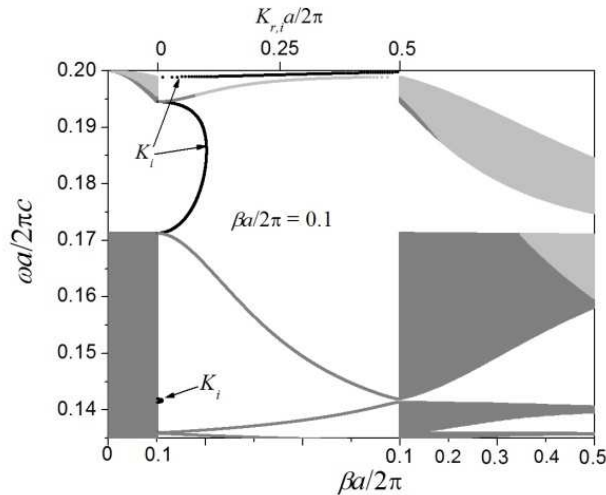


Figure 3. The same as Figure 2 for TE modes but showing explicitly the dispersion curve K vs. ω for $\beta a/2\pi = 0.1$. The Brillouin zone is defined by the range $0 < K < \pi/a$. The projected bands are artificially separated to introduce the Brillouin zone (upper scale in the figure). Inside an allowed band the Bloch wave vector is real and sweeps the entire Brillouin zone. Inside a forbidden gap the Bloch wave vector is complex.

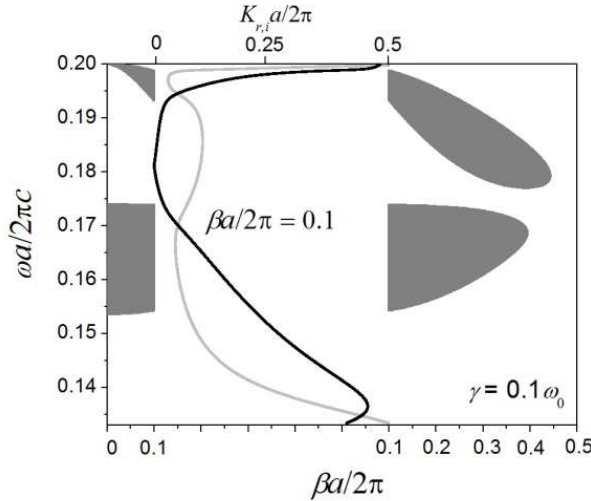


Figure 4. The same as Figure 3 but considering absorption mechanisms. The projected bands correspond to regions — over the complete plane of the figure — where the imaginary Bloch wave vector satisfies $K_i a/2\pi \leq 0.07$. To visualize the complex curve of dispersion at $\beta a/2\pi = 0.1$ we use the same upper scale for K_r and K_i .

inside the bulk bands and complex in the gaps. Now, in Figure 4 we take the losses into account to plot the same TE bands of Figure 3. We are using $\frac{\gamma}{\omega_0} = 0.1$. The gray extended regions correspond to waves with imaginary Bloch wave vector $\frac{K_i a}{2\pi} \leq 0.07$. Note that now strict separation between oscillatory and tunneling modes is not possible because the conditions $k_{zjR} = 0$ and $k_{zjI} \neq 0$ are not satisfied.

Plotting the projected bands has sense apparently only for lossless systems. In such a case the allowed and forbidden bands are clearly separated. As we mentioned above in the allowed bands the imaginary Bloch vector is zero and the real Bloch vector sweeps the Brillouin zone. On the other hand, in the forbidden bands the real Bloch vector keeps its value of the border of the zone and the imaginary component reaches its maximum value near the center of the band gap. Figure 4 shows that losses break with this condition — now the real and imaginary components of the Bloch vector have finite values in the entire frequency region. For plotting projected bands in presence of absorption we need to define the range of values of either the real or the imaginary wave vector of the modes that will be contained in them. This is completely necessary because the

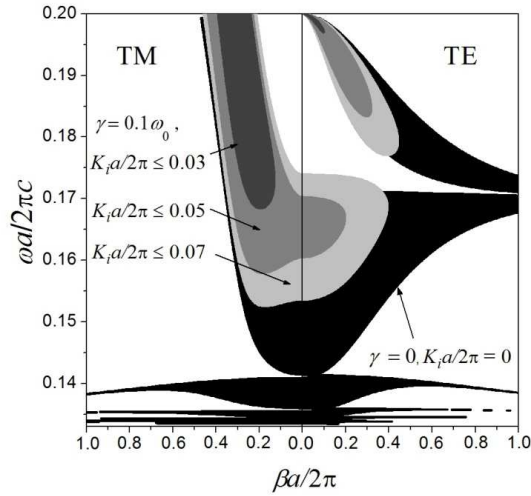


Figure 5. Complex projected photonic bands that show the effect of the absorption on the field penetration into the superlattice. The fields decay exponentially due to the imaginary Bloch wave vector component. As smaller is this component, larger is the field penetration.

absorption removes the pure forbidden and allowed frequency bands. We decided to select a maximum value K_{i0} and plot the solutions satisfying $K_i < K_{i0}$. We remind the reader that the penetration distance is inversely proportional to the imaginary vector: the larger the imaginary vector, the shorter the penetration distance. Thus, the bands for $K_i < K_{i0}$ contain modes that penetrate beyond the range of $z = 1/K_{i0}$.

In Figure 5 we present the general behavior for both TE and TM waves with the same absorption parameter $\frac{\gamma}{\omega_0} = 0.1$ for three limits of the imaginary Bloch wave vector; the bands in black are those for modes of infinite penetrability because absorption is zero for them. The three cases are: (a) $\frac{K_{ia}}{2\pi} \leq 0.07$. All the modes in these bands penetrate at least the distance $d \sim 2.27a$. In other words, in the light gray region of Figure 5 the amplitude of all the modes decays to $1/e$ of their reference value at distances equal or larger than $d = 2.27a$. Due to the existence of modes more penetrating than others, we proceed to find, step by step, the region of modes less sensitive to the losses — the modes of behavior similar to the behavior of the modes of the lossless situation. (b) $\frac{K_{ia}}{2\pi} \leq 0.05$. With this less imaginary wave vector the lowest penetration distance of the modes in

the gray regions of Figure 5 increases to $d \sim 3.18a$. Finally with (c) $\frac{K_i a}{2\pi} \leq 0.03$ the minimum penetration distance increases to $d \sim 5.3a$. The modes satisfying this condition are those of the dark gray zone in Figure 5. As we can see in Figure 5 absorption leaves shorter and shorter the region for the more penetrating modes. Note that regions are superimposed. The region described in (a) contains the regions of (b) and (c). Also the region (b) contains the region (c). Figure 5 is very important because it shows that the more penetrating modes have TE polarization. They lie in a small region of frequencies near the upper limit of the metamaterial regime. By comparing Figures 2 and 5 we conclude that these penetrating modes are of tunneling character.

So far we have presented general characteristics of the loss effect in the bulk bands for oblique propagation. Now we present transmission spectra through finite superlattice samples. The results are expected consistent with the corresponding bulk bands. In Figure 6 we present transmission spectra as function of the number of periods in the sample. The transfer matrix method is used for this calculation and the absorption coefficient is now $\frac{\gamma}{\omega_0} = 0.01$. We are varying the frequency of the TE incident wave with angle of incidence $\theta_i = 30^\circ$. [There exists a light-line of incidence, of slope $\frac{\omega}{\beta} = \frac{c}{\sin \theta_i}$, that lies inside the light-cone and superimposes on the corresponding projected bands. By varying the frequency of the incident wave we sweep all the (β, ω)

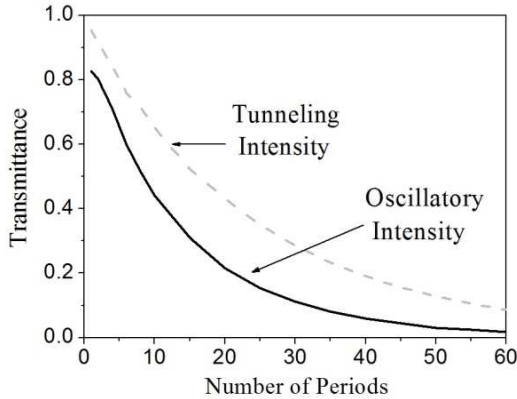


Figure 6. Peaks of transmittance through samples of finite number of periods. The waves are TE, the angle of incidence from air is 30° and $\gamma = 0.01\omega_0$. The transmitting medium is also air. The curves in this figure correspond to the maximum of transmission along the oscillatory and tunneling regions.

modes defined by this line and for each one of them we calculate the transmission intensity. Frequencies corresponding to the oscillatory and tunneling region are entirely swept]. Immediately we observe in Figure 6 that the transmission peaks of tunneling waves are higher independently of the number of layers. [It means that through the entire oscillatory region there is not a mode of higher penetration distance than the most penetrating mode in the tunneling region.] Note that this comparison is only quantitative, in terms of the penetration distance. It is not possible to compare tunneling and oscillatory modes of same frequency because they lay in different regimes. Specifically for a sample of 10 bilayers the frequencies and parallel wave vectors of the oscillatory and tunneling peaks are $\omega a/2\pi c = 0.1607$ ($f = 4.82$ GHz), $\beta a/2\pi = 0.08$ and, $\omega a/2\pi c = 0.1962$ ($f = 5.88$ GHz), $\beta a/2\pi = 0.098$, respectively. Because of the tunneling waves are more penetrating, in their frequency region there should be available a smaller imaginary Bloch wave vector than those in the oscillatory regime. In reality the result of Figure 6 is already inferred from Figure 5. With $\beta a/2\pi$ lower than 0.1 the smaller imaginary Bloch wave vector exist in the upper band, precisely in the tunneling region (See Figure 5).

To complement the analysis, we now present the field amplitudes inside the periodic sample (when reflectance is calculated) for the two types of modes here discussed.

We plot in Figure 7 the field profiles inside a sample of 20 periods. Panels (a) and (b) are for oscillatory and tunneling waves, respectively. The frequencies and angle of incidence correspond to the modes of optimum transmission that gave place to Figure 6 at $z/a = 20$. For the oscillatory mode the field amplitude oscillates from cell to cell with larger changes, in average, in the LHM layers. Note that local minima and maxima amplitudes can exist inside the LHM layers ($z = 6a$, $z = 16a$, etc..) In general, due to the boundary conditions, the field profile presents a structure of peaks with maxima and minima just at the interfaces between the layers (at any interface the fields $E_x \propto \varepsilon^{-1} \partial H_y / \partial z$ and $H_y \propto \mu^{-1} \partial E_x / \partial z$ are continuous; because of the change of sign of ε and μ from layer to layer, the derivative of the fields must change sign through the interfaces). On the other hand, for the tunneling mode the larger changes of amplitude occur in the air layers where the fields oscillate because the corresponding mode lies inside the light-cone. In the LHM the forward and backward evanescent fields overlap giving place to almost constant amplitude through each LHM layer.

The loss effect on the wave propagation is clearly observed in Figure 7. As we mentioned previously the decay distance of the fields inside the superlattice is defined by the imaginary Bloch wave

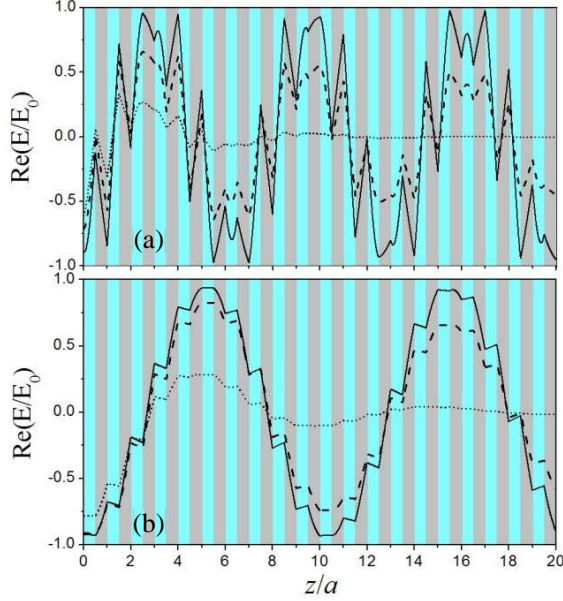


Figure 7. TE field distribution in a sample of 20 bilayers. The wave is incident from air with angle of incidence $\theta_i = 30^\circ$. Solid line, dashed line and dotted line correspond to absorption parameters $\gamma = 0$, $\gamma = 0.01\omega_0$ and $\gamma = 0.1\omega_0$, respectively. (a) Oscillatory mode: $\omega a/2\pi c = 0.1607$ and $\beta a/2\pi = 0.08$, (b) Tunneling mode: $\omega a/2\pi c = 0.1962$ and $\beta a/2\pi = 0.098$.

vector K_i that depends on the position of the mode in the bulk band. The two modes of Figure 7 have given optimum transmission in the oscillatory and tunneling regions, respectively, when absorption is $\frac{\gamma}{\omega_0} = 0.01$ (See Figure 6 for a sample of 20 bilayers). From Figure 7 we deduce that even with absorption as high as $\frac{\gamma}{\omega_0} = 0.1$ it is expected larger transmittance by tunneling waves in a sample of 10 cells. At this depth and with this absorption, the amplitude of the oscillatory mode is $\text{Re}(E/E_0) = 0.025$ while for the tunneling waves this rate is $\text{Re}(E/E_0) = 0.1$.

4. FINAL REMARKS AND CONCLUSIONS

It is important to remark that for describing the wave propagation in lossy LHM/RHM superlattices, one requires to introduce complex Bloch wave vectors. Consequently, it is necessary to redefine the concept of projected band establishing an additional criterion for

displaying them. We have chosen the magnitude of the imaginary K_i as a good parameter for plotting spots on the plane (β, ω) corresponding to photonic modes of defined penetrability. With this condition we were able to exclude the less penetrating modes focusing the analysis on those of larger penetration. It is interesting that for incident light from vacuum the most penetrating modes into the LHM/RHM superlattice are TE polarized; they are contained in a tiny spot near the upper limit of the metamaterial regime and are tunneling modes in character.

In conclusion we have studied the photonic modes in a lossy and dispersive LHM/RHM superlattice. We were interested in the modes that can be excited by light which is incident from vacuum. Inside the light-cone of vacuum we identify (via the light-curve of the LHM) the oscillatory and tunneling modes in the non-lossy projected photonic bands. In order to take into account absorption phenomena, we have established a strategy for plotting the projected bands. By choosing a maximum value for the imaginary Bloch wave vector K_i we can find the regions in the plane (β, ω) corresponding to modes with equal or larger penetration than that defined by K_i .

As is expected, the photonic bands are highly sensitive to the losses. Even when absorption affects similarly the two types of modes, we have presented numerical evidence that the intensity of the energy transmitted by tunneling modes is the larger one. This result is independent of the number of cells in the sample. Previous works have demonstrated field amplification of evanescent waves by LHM/RHM structures. The tunneling modes here presented are characterized by evanescent and oscillatory waves in the LHM and RHM, respectively. Our conclusion is that evanescent and oscillatory waves in subsequent LHM-RHM layers couple more favorably to increase the penetration length into the superlattice.

Finally, we have shown numerically the existence of a projected band without modes at $\beta = 0$. The effect is completely associated to the metamaterial regime because, in general, for one dimensional photonic crystals of dielectric or metallic components (RHM constituents) any projected band has acoustic type modes at $\beta = 0$.

ACKNOWLEDGMENT

This work was supported by Consejo Nacional de Ciencia y Tecnología, México, Grant No. 24051 and by Subsecretaría de Educación Superior e Investigación Científica, México, Programa de Mejoramiento del Profesorado, Redes Temáticas de Cuerpos Académicos, Grant FOFM-2008.

REFERENCES

1. Veselago, V. G., "Electrodynamics of substances with simultaneously negative values of ε and μ ," *Sov. Phys. Usp.*, Vol. 10, 509–514, 1968.
2. Agranovich, V. M. and Y. N. Garstein, "Spatial dispersion and negative refraction of light," *Physics-Uspokhi*, Vol. 49, 1029–1044, 2006.
3. Shelby, R. A., D. R. Smith, and S. Schultz, "Experimental verification of a negative refractive index of refraction," *Science*, Vol. 292, 77, 2001.
4. Pendry, J. B., "Negative refraction makes a perfect lens," *Phys. Rev. Lett.*, Vol. 85, 3966, 2000.
5. Smith, D. R., W. J. Padilla, D. C. Vier, S. C. Nemat-Nasser, and S. Schultz, "Composite medium with simultaneously negative permeability and permittivity," *Phys. Rev. Lett.*, Vol. 84, 4184–4187, 2000.
6. Shelby, R. A., D. R. Smith, S. C. Nemat-Nasser, and S. Schultz, "Microwave transmission through a two dimensional, isotropic, left-handed metamaterial," *Appl. Phys. Lett.*, Vol. 78, 489–491, 2001.
7. Pandey, G. N., K. B. Thapa, S. K. Srivastava, and S. P. Ojha, "Band structures and abnormal behavior of one dimensional photonic crystal containing negative index materials," *Progress In Electromagnetic Research M*, Vol. 2, 15–36, 2008.
8. Srivastava, S. K. and S. P. Ojha, "Enhancement of omnidirectional reflection bands in one-dimensional photonic crystals with left-handed materials," *Progress In Electromagnetic Research*, Vol. 68, 91–111, 2007.
9. Wang, Z.-Y., X.-M. Chen, X.-Q. He, S.-L. Fan, and W.-Z. Chan, "Photonic crystal narrow filters with negative refractive index structural defects," *Progress In Electromagnetic Research*, Vol. 80, 421–430, 2008.
10. Zhang, Z. M. and C. J. Fu, "Unusual photon tunneling in the presence of a layer with a negative refractive index," *Appl. Phys. Lett.*, Vol. 80, 1097–1099, 2002.
11. Kim, K. Y., "Photon tunneling in composite layers of negative- and positive-index media," *Phys. Rev. E*, Vol. 70, 047603, 2004.
12. Li, J. S., L. Zhou, C. T. Chan, and P. Sheng, "Photonic band gap from a stack of positive and negative index materials," *Phys. Rev. Lett.*, Vol. 90, 083901, 2003.

13. Yuan, Y., L. Ran, J. Huangfu, H. Chen, L. Shen, and J. A. Kong, "Experimental verification of zero order bandgap in a layered stack of left-handed and right-handed materials," *Optics Express*, Vol. 14, 2220–2227, 2006.
14. Wu, L., S. He, and L. Shen, "Band structure for a one-dimensional photonic crystal containing left-handed materials," *Phys. Rev. B*, Vol. 67, 235103, 2003.
15. García, N. and M. Nieto-Vesperinas, "Left-handed materials do not make a perfect lens," *Phys. Rev. Lett.*, Vol. 88, 207403, 2002.
16. Rao, X. S. and C. K. Ong, "Amplifications of evanescent waves in a lossy left-handed material slab," *Phys. Rev. B*, Vol. 68, 113103, 2003.
17. De Dios-Leyva, M. and J. A. Leyva-Galano, "Influence of absorption on the zero-n gap in one dimensional photonic crystals with left-handed materials," *Phys. Rev. B*, Vol. 78, 115106, 2008.
18. Zhou, X. and G. Hu, "Total transmission condition for photon tunneling in a layered structure with metamaterials," *J. Opt. A: Pure Appl. Opt.*, Vol. 9, 60–65, 2007.
19. Markos, P. and C. M. Soukoulis, "Transmission studies of left-handed material," *Phys. Rev. B*, Vol. 65, 033401, 2001.
20. Smith, D. R. and N. Kroll, "Negative refractive index in left-handed materials," *Phys. Rev. Lett.*, Vol. 85, 2933, 2000.
21. Pacheco, Jr., J., T. M. Grzegorzcyk, B.-I. Wu, Y. Zhang, and J. A. Kong, "Power propagation in homogeneous isotropic frequency-dispersive left-handed media," *Phys. Rev. Lett.*, Vol. 89, 257401, 2002.
22. Koschny, T., M. Kafesaki, E. N. Economou, and C. M. Soukoulis, "Effective medium theory of left-handed materials," *Phys. Rev. Lett.*, Vol. 93, 107402, 2004.
23. Caloz, C. and T. Itoh, *Electromagnetic Metamaterial: Transmission Line Theory and Microwave Applications*, John Wiley & Sons, Inc., 2006.
24. Gupta, S. D., R. Arun, and G. S. Agarwal, "Subluminal to superluminal propagation in a left-handed medium," *Phys. Rev. B*, Vol. 69, 113104, 2000.
25. Villa-Villa, F., J. A. Gaspar-Armenta, and A. Mendoza-Suárez, "Surface modes in one dimensional photonic crystals that include left handed materials," *Journal of Electromagnetic Waves and Applications*, Vol. 21, No. 4, 485–499, 2007.